Interaction Between a Low-Temperature Plasma and Graphene: An *in situ* Raman Thermometry Study

Carla Berrospe-Rodriguez,[1] Joseph Schwan,[1] Giorgio Nava,[1] Fariborz Kargar,[2] Alexander A. Balandin,[2,3] and Lorenzo Mangolini[1,3,*]

[1] *Department of Mechanical Engineering, University of California, Riverside, 900 University Ave., Riverside, California 92521, USA*

[2] *Department of Electrical and Computer Engineering, University of California, Riverside, 900 University Ave., Riverside, California 92521, USA*

[3] *Materials Science and Engineering Program, University of California, Riverside, 900 University Ave., Riverside, California 92521, USA*

(Received 19 October 2020; revised 14 December 2020; accepted 19 January 2021; published 8 February 2021)

The localized release of energy at the surface of plasma-exposed materials plays a crucial role in many plasma-driven processes. Unfortunately, the interaction between low-temperature plasmas and surfaces is both poorly understood and difficult to characterize. Here, we use Raman thermometry to measure the temperature of graphene during plasma exposure. We observe a significant increase in the graphene temperature even for modest input plasma powers. These results suggest that two-dimensional materials are effective surface probes for the quantitative characterization of plasma-induced heating effects and for further investigation of the plasma-surface interaction.

DOI: 10.1103/PhysRevApplied.15.024018

I. INTRODUCTION

Low-temperature, nonthermal plasma are routinely utilized to activate a wide range of surface reactions. These include well-established processes such as reactive ion etching [1,2] as well as more recent developments, such as plasma-enabled atomic layer deposition [3,4], plasma-driven heterogeneous chemistry [5–7] (commonly referred to as plasma catalysis), and plasma processing of two-dimensional materials [8–12]. It is well known that exposure to low-temperature plasmas can accelerate the kinetics of many surface processes. For instance, Kim et al. [5] have reported the efficient decomposition of methane over nickel catalyst at a reduced temperature when exposed to a dielectric barrier discharge (DBD) compared with a thermally driven reaction. Liu et al. [9] have demonstrated the nucleation and growth of hexagonal boron nitride (hBN) from a molecular precursor at a temperature as low as 500 °C when exposed to an atmospheric-pressure nonthermal plasma, whereas 800 °C is needed for a thermally driven process. Consistent with these findings, Beaudette et al. [13] have recently shown the plasma-enhanced chemical vapor deposition (CVD) of high-quality MoS_2 films at 500 °C, which is considerably lower than what is otherwise needed for the heat-only case. The enhancement of the kinetics of surface reactions under plasma exposure is due to several effects, including the preexcitation of molecules in the gas phase and the momentum transfer to the surface induced by ion bombardment. Plasma-produced radicals and metastables also recombine and react at plasma-exposed surfaces, often following an exothermic reaction path. This results in the localized release of energy at plasma exposed surfaces, a phenomenon commonly referred to as plasma heating. As an example, the recombination of plasma-produced atomic hydrogen at the surface of nanoparticles in dusty plasmas induces substantial heating [14] and enables the processing of refractory materials [15,16]. Nanoparticle temperature measurements confirm the significant role played by plasma heating for the case of dusty plasmas [17–20]. It should be noted that the low rate of heat dissipation from the particles to the background gas in these scenarios leads to a significant temperature increases. On the other hand, the extent of plasma heating effects for the case of an extended (semi-infinite) substrate (as opposed to small particles dispersed in the plasma) is both under-characterized and actively debated. This is largely due to the lack of quantitative measurements. Walton et al. [21] have recently addressed this same issue by performing pump-probe time-domain thermoreflectance measurements for the case of a metallic films exposed to a low-temperature plasma, confirming the presence of localized plasma-induced heating. Although elegant, this work relies on specialized equipment that may not be readily available to many research groups.

*lmangolini@engr.ucr.edu

Here, we describe an approach towards the quantification of plasma-induced surface heating which relies on measuring the temperature of an atomically thin material while exposed to a low-temperature plasma. In other words, we use a two-dimensional material as a surface-sensitive temperature probe. We focus on graphene because of its high Raman cross-section, its clear and well-characterized Raman signature, and because it is atomically thin, ensuring that a surface-specific temperature measurement is performed. This is necessary because plasma-induced heating is inherently localized at the plasma-exposed surface.

Graphene has been widely studied during the last two decades. Graphene has proven to be a great thermal conductor with high electron mobility and chemically robustness [22–29]. These qualities have led to the implementation of graphene in many fields such as electrochemical energy conversion and storage [30–32], sensing [33,34], graphene-based catalysis [35–37], postsilicon electronics [38,39], and thermal interface materials for heat management and electromagnetic interference shielding [40–42], among countless others [43–47].

Here we use graphene grown by CVD onto a copper foil substrate. The temperature of the graphene surface exposed to the plasma is obtained by the principle of Raman thermometry, where the signal strength of the G Raman band at the Stokes and anti-Stokes positions are measured simultaneously. Raman thermometry offers a noncontact, spatially resolved approach to temperature measurement, and for this reason it has been adopted by several research groups [48,49]. To calibrate our measurements, a vacuum chamber with heating capabilities is used to bring the graphene to a desired initial temperature, before plasma exposure. When the chamber is heated to 200 °C, exposure to a radiofrequency (RF) argon plasma immediately raises the temperature to approximately 350 °C. The temperature increase is independent of substrate temperature and linearly dependent on the plasma input power. In addition, a simple heat transfer model is developed using COMSOL MULTIPHYSICS to rule out the possibility that the temperature increment is simply due to gas heating by the plasma. The temperature of the multilayered graphene presents a significant dependence on the plasma composition, where higher temperature is observed in pure argon rather than hydrogen-diluted argon gas. Finally, we show evidence of anisotropic etching by means of hydrogenation, where the increased hydrogen concentration leads to the reduction in the size of the graphene domains, and to an increased disorder in the material structure. This study highlights the untapped potential of graphene and other two-dimensional materials as probes for the investigation of poorly understood plasma-related phenomena.

II. METHODS

Figure 1(a) shows a schematic of the set-up used in this study. The system consists of a high-temperature reaction vacuum chamber (HVC-DRM-5 from Harrick Scientific Products), where a tubelike capacitively coupled nonthermal plasma reactor [7.5 mm long, 5.16 mm inner diameter (ID), 10 mm outer diameter (OD), borosilicate glass] is mounted onto one of the chamber flanges. A photograph of the assembly can be found in the Supplemental Material, Fig. S1 [50]. The plasma is powered by a 13.56 MHz RF power supply. The RF voltage is applied between one copper ring electrode wrapped around the plasma tube and the grounded reaction chamber. The plasma expands in the chamber impinging onto the graphene-coated substrate. Two copper ring electrodes are wrapped around the plasma tube, and a plasma jet extends from the tube into

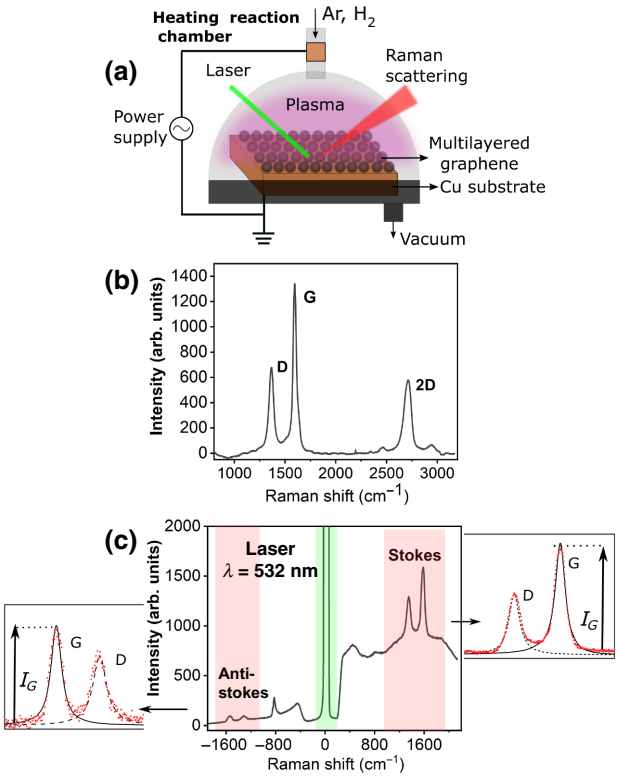

FIG. 1. (a) Schematic of the reaction chamber for *in situ* Raman study. (b) Raman spectrum of multilayered graphene pristine sample collected at $\lambda = 532$ nm. The typical D (± 1332 cm^{-1}) and G (± 1598 cm^{-1}) peaks from carbonaceous materials and the two-dimensional peak (± 2600 cm^{-1}), which has the largest intensity in a single-layer graphene, but it significantly reduces in multilayer graphene, are shown. (c) Central image: Stokes and anti-Stokes *in situ* Raman spectral lines from a sample heated up to 600 °C during a 12-W plasma impinging at the graphene surface. Side images: Signal fitting encompassing a Lorentzian peak for the D component, a BWF line shape for the G component for: anti-Stokes (left) and Stokes (right) modes.

the small vacuum chamber, impinging onto the graphene-coated substrate. Graphene is grown on copper foils heated to 1030 °C using a low-pressure CVD of carbon using a mixture of methane and hydrogen. The copper substrate is cooled down from 1030 °C to room temperature in 10 h by carefully controlling the cooling rate. The details of the growth process are described in Refs. [51,52]. The CVD grown multilayered graphene film (MGF) on copper foil is placed on top of the temperature controlled heater. A gas mixture comprising Ar and H_2 at different concentrations (from 100% Ar to 80% Ar – 20% H_2) is supplied at different flow rates (from 15 to 40 sccm). The chamber pressure is 13 Torr.

The *in situ* Raman scattering system has been developed to acquire the Stokes and anti-Stokes D and G peaks from the MGF sample simultaneously. The optical system comprises of a continuous wave laser at $\lambda = 532$ nm with a laser power up to 1 W (4×10^5 mW/cm^2, spot size of 500 μm). The scattered light is collected and focused to a visible-near-infrared (VIS-NIR) monochromator (Acton Spectra Pro, Princeton Instruments) and captured by a CCD camera located at the exit slit of the monochromator. Figure 1(b) shows the Raman spectrum of the graphene samples used for this study. Signatures from the well-known D, G, and 2D peaks of graphene are shown. The laser excitation is mechanically chopped and the acquisition system is synchronized to precisely remove the emission from the discharge. A detailed description of the optical system and the signal acquisition procedure can be found in the Supplemental Material, Fig. S2 [53].

A spectral deconvolution is performed to obtain the intensity of the Raman peaks by a fitting routine. A Lorentzian function is used for the D component and a Breit Wigner Fano (BWF) function for the G component [54]. This is shown in the left image of Fig. 1(c) for the anti-Stokes line and the right image for the Stokes line. The temperature of the samples is calculated based on the temperature-dependent population of vibrational modes:

$$\frac{I_s}{I_{\text{as}}} = \left(\frac{\lambda_s}{\lambda_{as}}\right)^4 e^{-\frac{h\upsilon}{kT}} \tag{1}$$

where h is the Plank's constant, k is the Boltzmann's constant, T is temperature, υ is the Raman frequency, I_s, λ_s and I_{as}, λ_{as} are the peaks intensities and wavelengths of the Stokes and anti-Stokes lines, respectively. It is important to stress that Eq. (1) is valid for nonresonant Raman scattering. Although both G and D bands in graphene arise from a resonance process [55], this does not appear to impair the validity of Eq. (1) in our study. We attribute this observation to the absence of singularities in the electronic structure of our multilayer graphene samples [56], making the resonance effect on the Stokes to anti-Stokes ratio negligible.

III. RESULTS AND DISCUSSION

As a first step, we simultaneously acquire the Stokes and anti-Stokes spectra of a MGF sample while the substrate temperature is linearly increased from 200 °C to 600 °C. This study is performed with and without the Ar-H_2 plasma (90% Ar and 10% H_2, 30 sccm total) impinging onto the graphene surface. As expected from the increase in the thermal population of the vibrational modes, an increase of the anti-Stokes signal intensity is observed [see Fig. 2(a)] as the substrate temperature is raised. The intensities of the G peaks are obtained by fitting the recorded spectra with the routine described above, then the temperature of the multilayer graphene is calculated with Eq. (1). Figure 2(b) shows the surface temperature T_{SFC} as a function of the substrate temperature for both conditions, without plasma and with a 12 W plasma. Regardless of the substrate temperature, we observe an increment $\Delta T = 68 \pm 5$ °C as a result of exposure to the Ar-H_2 plasma. This outcome confirms the increase in surface temperature induced by the exposure to the plasma. However, further studies were carried out to discard the possibility that this increase in surface temperature is simply due to heating of the gas by the plasma.

We use COMSOL MULTIPHYSICS to model the heat-transfer occurring in our system. The geometry is simplified in the model to reduce computational load as is shown in Fig. 3(a). The system is modeled in a two-dimensional

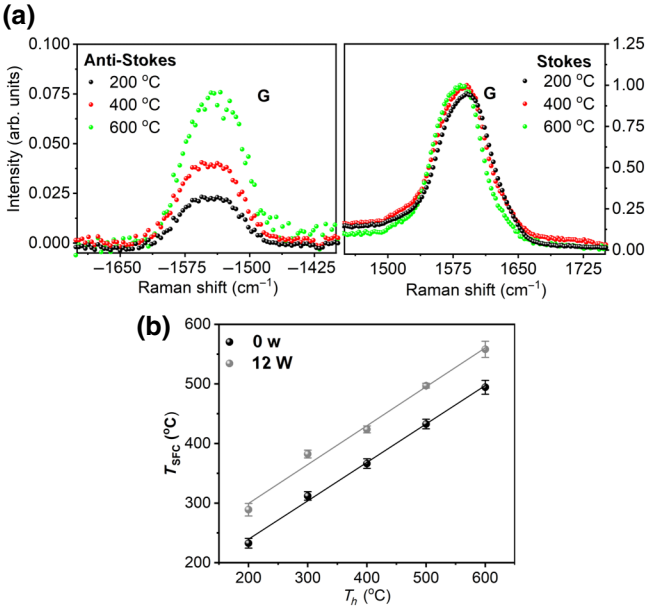

FIG. 2. (a) Anti-Stokes and Stokes *in situ* Raman G peak of multilayered graphene heated up at substrate temperature or 200 °C, 400 °C, and 600 °C, with plasma off, with a total flow of 30 sccm of an argon-hydrogen mixture. (b) Temperature at the graphene surface as a function of chamber temperature with and without a 12-W Ar-H_2 plasma, obtained by Raman thermometry.

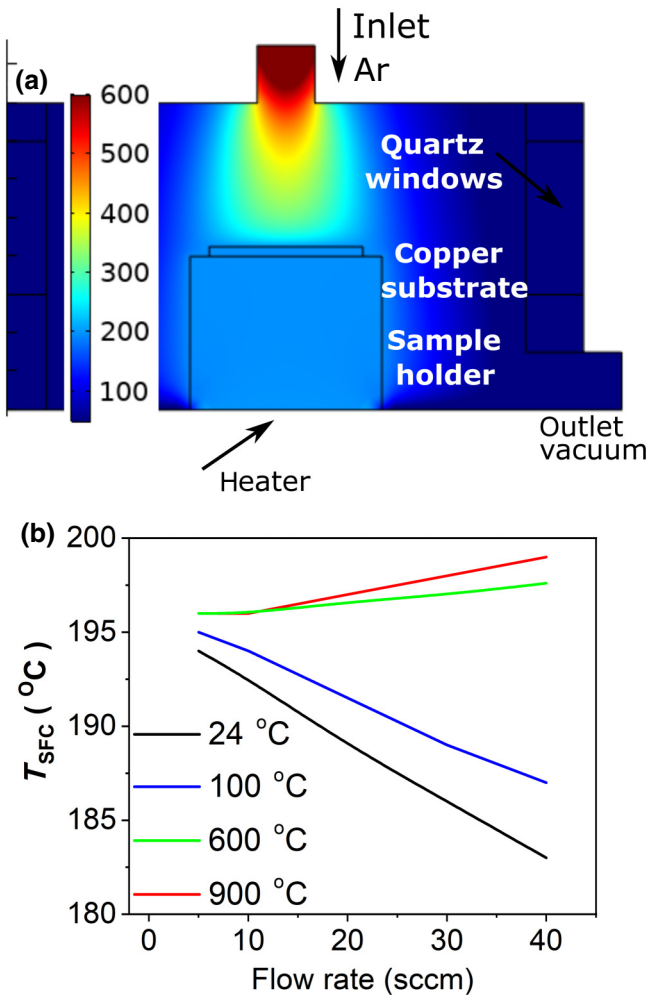

FIG. 3. (a) Heat transfer computer model in COMSOL MULTIPHYSICS to study the temperature profile at the substrate surface due to gas heating. (b) Calculated surface temperatures as a function of the flow rate for different gas temperatures.

geometry. An initial temperature of 200 °C is set at the bottom of the stainless-steel sample holder heater. Argon gas is added through the top inlet, where its temperature is set, and evacuated at a bottom-right outlet. While in the experiments the gas is injected into the plasma at room temperature, in the calculations the inlet gas temperature is varied to simulate any potential gas heating induced by the plasma, and to investigate its effect onto the substrate surface temperature. The temperature at the substrate surface T_{SFC} for different gas temperatures and different flow rates (from 0 to 40 sccm) is evaluated using this computational approach. Figure 3(b) shows the results from the computational model for different gas flow rates and for inlet gas temperatures ranging from room temperature to up to 900 °C.

For all these conditions, we observe only a minor deviation of T_{SFC} from the substrate base temperature of 200 °C. The surface temperature is quite close to 200 °C even when the gas temperature is 900 °C. This is due to the large heat transfer rate through the solid substrate and the poor convective heat transfer in the gas phase, especially at these low operating pressures. Detailed information about the computer model is described in Sec. S.3 of the Supplemental Material [57]. Moreover, the increase in graphene temperature upon plasma exposure is constant at a given plasma input power and does not depend on the substrate temperature, as shown in Fig. 3(b). This again rules out a gas heating effect, because in that case the heat flux to the surface would be proportional to the temperature difference between gas and substrate. In the limiting case in which the substrate temperature matches the gas temperature, there would be no heat transfer and no temperature increase at the surface. We instead observe the same surface temperature increase of roughly 70 °C even when the substrate temperature is 600 °C. It is highly unlikely that the gas temperature is considerably higher than 600 °C. To confirm that, we have estimated the magnitude of gas heating that is induced by the plasma via collisions between free electrons and background gas. The rate of gas heating is deduced using a commonly utilized Boltzmann solver, BOLSIG+ [58]. This freeware software provides a solution of the electron transport equation in an ionized gas, and predicts the amount of energy transferred from the electron gas to the background gas. Using the same gas composition as in the results shown in Fig. 2 (10% H_2 – 90% Ar), and assuming realistic values of plasma parameters (plasma density of 10^{10} cm^3 and electron temperature of 2 eV), we calculate a gas temperature of 50 °C at the exit of the plasma volume. Heating of the gas by the plasma cannot therefore explain the measured increase in surface temperature [shown in Fig. 2(b)], especially for the case in which the substrate temperature largely exceeds the gas temperature (as high as 600 °C). The increase in graphene temperature is instead induced by the localized release of energy at the surface in contact with the plasma.

A study is performed on the influence of plasma composition on graphene surface temperatures. Different Ar-H_2 gas concentration plasmas, from 0% to 20% of hydrogen dilution, are investigated in our *in situ* Raman system. First, the plasma optical emission spectra (OES) of all the studied concentrations at 10 W power are acquired, as is shown in Sec. S.4 of the Supplemental Material [59]. The peak intensities in the 640–970 nm range diminish as the hydrogen concentration increases. Figure 4(a) shows the integrated area over all the OES peaks as a function of the H_2 percentage. As can be observed, the plasma intensity strongly decreases as the hydrogen content increases. Pristine MGF samples with an initial temperature of 200 °C are exposed to each of these Ar-H_2 plasmas and the temperature of the surface is measured via Raman thermometry as described previously. Figure 4(b) shows the variation

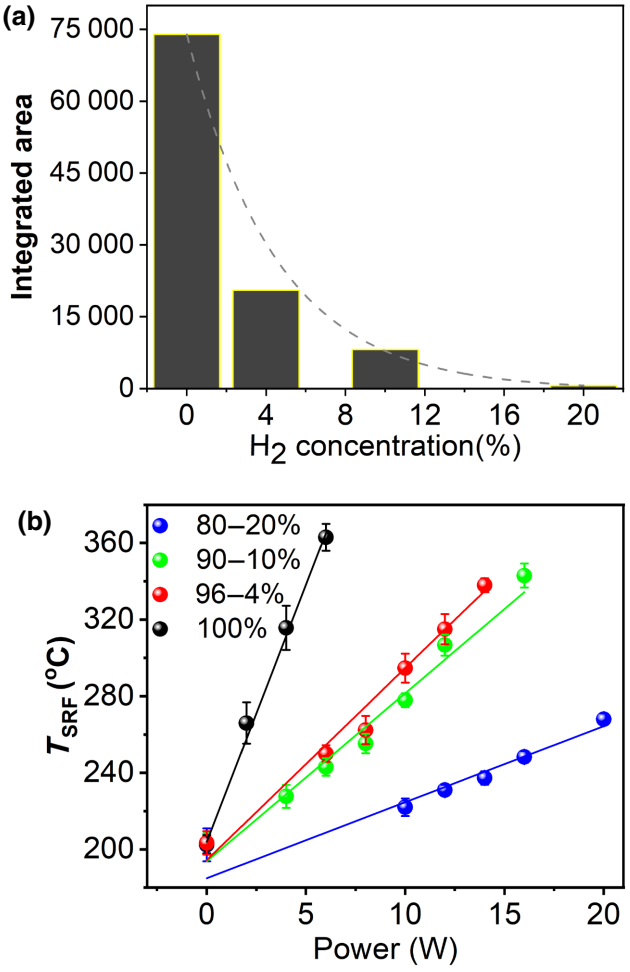

FIG. 4. (a) Integrated area of OES peaks as a function of H_2 dilution concentration in Ar. (b) Temperature at the graphene surface as a function of plasma coupled power for different Ar-H_2 gas concentrations.

in surface temperature T_{SFC} as a function of gas composition and input plasma power. A strong decrease is observed as the H_2 concentration increases. A maximum T_{SFC} of 365 °C is reached for 100% Ar plasma even with only 6 W of input RF power, whereas 20 W of an 80% Ar − 20% H_2 plasma are needed to reach 270 °C, an increment of only 70 °C from the initial temperature. We have found that it is not possible to sustain the plasma below 10 W for this gas composition.

These results confirm that surface heating is strongly dependent on gas composition. The addition of hydrogen has a quenching effect on the plasma, reducing the intensity of the discharge [consistent with the data shown in Fig. 4(b)] and as a consequence decreasing the energy released at the plasma-exposed graphene surface.

Finally, we discuss how plasma exposure affects the structural properties of the graphene layers. Figure 5(a), left, reports a scanning electron microscopy (SEM)

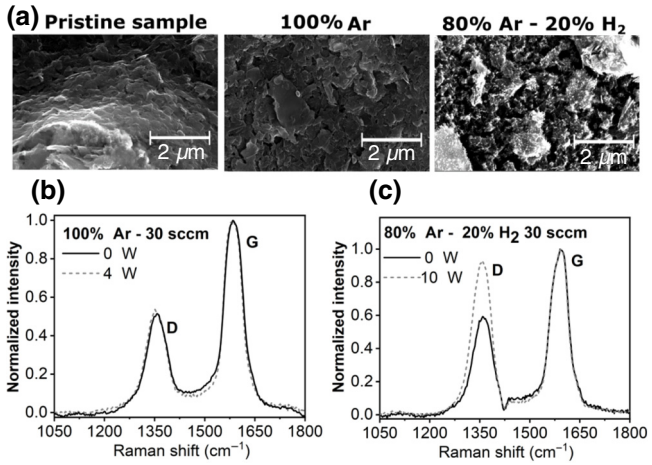

FIG. 5. (a) SEM micrograph of graphene surfaces. Left: Pristine sample. Center: After 5 min of 100% Ar plasma exposure. Right: After 5 min of 80% Ar − 20% H_2 plasma exposure. (b) Raman D and G peaks during no plasma and 100% Ar plasma exposure. (c) Raman D and G peaks during no plasma and 80% Ar − 20% H_2 plasma exposure.

top-view micrograph of a multilayered graphene pristine sample, where a continuous morphology film is observed. We estimated the number of graphene layers to be around 10, based on the method suggested by Bellani et al. [60], as is shown in Sec. S.5 of the Supplemental Material [61]. After 5 min of 100% argon plasma exposure, the continuous film peels off slightly leaving slightly smaller graphene structures, as shown in Fig. 5(a). We observe no significant change in the I_D/I_G intensity ratio, indicating no significant modification in the graphene structure [see Fig. 5(b)]. However, upon the addition of hydrogen to the plasma, the graphene structure becomes more disordered, as shown in the right panel of Fig. 5(a). The presence of defects after exposure to the argon-hydrogen plasma is confirmed by the Raman spectra shown in Fig. 5(c). As the hydrogen concentration in the gas increases, the I_D/I_G intensity ratio increases as well. For 20% hydrogen, I_D/I_G reaches a value of 0.93 after a 5 min plasma treatment, consistent with an increased density of defects [62]. These results are consistent with plasma anisotropic etching at preexisting point defects by means of hydrogenation, which is a preferential process for multilayer films rather than single layer graphene, as was reported previously [63].

IV. CONCLUSIONS

In summary, we have utilized graphene as a surface probe to investigate the low-temperature plasma-surface interaction. *In situ* Raman thermometry confirms that surface temperature considerably exceeds substrate temperature [by as much as 150 °C even at moderate plasma input powers, as shown in Fig. 3(b)]. The surface temperature increase is independent of substrate temperature and

strongly dependent on gas-phase composition and plasma input power. This is consistent with the localized release of energy at the surface of the material owing to the exposure to plasma-produced active species. This is further confirmed by computational results which conclusively rule out that the plasma simply acts as a gas heating source.

It is well known that plasma activation allows to perform various processes at a reduced thermal load. A variety of mechanism contribute to this effect, and the plasma-material interaction is notoriously complex and not well understood. The results reported here are significant because (a) even a seemingly small degree of surface heating can drastically increase surface reaction rates owing to their exponential dependence on temperature and (b) graphene and other two-dimensional materials may be ideal probes for *in situ*, *in operando* monitoring of surface temperature in plasma-driven processes.

In addition, we have shown that *in situ*, *in operando* Raman is a useful tool for monitoring structural changes in two-dimensional materials during plasma processing. We advocate for a more widespread utilization of this technique, particularly for the study of graphene and other two-dimensional materials which are promising and increasingly relevant in applications ranging from microelectronics to sensing and electrochemistry.

ACKNOWLEDGMENTS

This work was supported by the U.S. Army Research Office under Grant No. W911NF-17-1-0340 and the UC MEXUS-CONACYT Postdoctoral Fellowship Program 2019-2020. A.A.B. acknowledges support of the National Science Foundation (NSF) Designing Materials to Revolutionize and Engineer our Future (DMREF) via DMR-1921958, and the Semiconductor Research Corporation (SRC) contract 2018-NM-2796.

[1] G. S. Oehrlein and Y. H. Lee, Reactive ion etching related Si surface residues and subsurface damage: Their relationship to fundamental etching mechanisms, J. Vac. Sci. Technol., A **5**, 1585 (1987).

[2] J. W. Coburn, Role of ions in reactive ion etching, J. Vac. Sci. Technol., A **12**, 1417 (1994).

[3] R. J. Gasvoda, Z. Zhang, S. Wang, E. A. Hudson, and S. Agarwal, Etch selectivity during plasma-assisted etching of SiO_2 and SiNx: Transitioning from reactive ion etching to atomic layer etching, J. Vac. Sci. Technol., A **38**, 050803 (2020).

[4] V. R. Rai, V. Vandalon, and S. Agarwal, Surface reaction mechanisms during ozone and oxygen plasma assisted atomic layer deposition of aluminum oxide, Langmuir **26**, 13732 (2010).

[5] J. Kim, M. S. Abbott, D. B. Go, and J. C. Hicks, Enhancing C – H bond activation of methane via temperature-controlled, catalyst–plasma interactions, ACS Energy Lett. **1**, 94 (2016).

[6] P. Mehta, P. Barboun, F. A. Herrera, J. Kim, P. Rumbach, D. B. Go, J. C. Hicks, and W. F. Schneider, Overcoming ammonia synthesis scaling relations with plasma-enabled catalysis, Nat. Catal. **1**, 269 (2018).

[7] T. Nozaki, N. Muto, S. Kado, and K. Okazaki, Dissociation of vibrationally excited methane on Ni catalyst: Part 1. Application to methane steam reforming, Catal. Today **89**, 57 (2004).

[8] H. M. Kim, H.-H. Sun, I. Belharouak, A. Manthiram, and Y.-K. Sun, An alternative approach to enhance the performance of high sulfur-loading electrodes for Li – S batteries, ACS Energy Lett. **1**, 136 (2016).

[9] T. Liu, K. Premasiri, Y. Sui, X. Zhan, H. A. B. Mustafa, O. Akkus, C. A. Zorman, X. P. A. Gao, and R. M. Sankaran, Direct, transfer-free growth of large-area hexagonal boron nitride films by plasma-enhanced chemical film conversion (PECFC) of printable, solution-processed ammonia borane, ACS Appl. Mater. Interfaces **10**, 43936 (2018).

[10] H. Nan, R. Zhou, X. Gu, S. Xiao, and K. Ostrikov, Recent advances in plasma modification of 2D transition metal dichalcogenides, Nanoscale **11**, 19202 (2019).

[11] T. Liu, X. Liu, S. Bhattacharya, Z. Ye, R. He, X. P. A. Gao, R. Akolkar, and R. M. Sankaran, Plasma-Induced fabrication and straining of MoS_2 films for the hydrogen evolution reaction, ACS Appl. Energy Mater. **2**, 5162 (2019).

[12] I. Childres, L. A. Jauregui, J. Tian, and Y. P. Chen, Effect of oxygen plasma etching on graphene studied using Raman spectroscopy and electronic transport measurements, New J. Phys. **13**, 025008 (2011).

[13] C. A. Beaudette, J. T. Held, K. A. Mkhoyan, and U. R. Kortshagen, Nonthermal plasma-enhanced chemical vapor deposition of two-dimensional molybdenum disulfide, ACS Omega **5**, 21853 (2020).

[14] L. Mangolini and U. Kortshagen, Selective nanoparticle heating: Another form of nonequilibrium in dusty plasmas, Phys. Rev. E **79**, 026405 (2009).

[15] D. Coleman, T. Lopez, O. Yasar-Inceoglu, and L. Mangolini, Hollow silicon carbide nanoparticles from a nonthermal plasma process, J. Appl. Phys. **117**, 193301 (2015).

[16] S. Exarhos, A. Alvarez-Barragan, E. Aytan, A. A. Balandin, and L. Mangolini, Plasmonic core–shell zirconium nitride–silicon oxynitride nanoparticles, ACS Energy Lett. **3**, 2349 (2018).

[17] G. Swinkels, H. Kersten, H. Deutsch, and G. M. W. Kroesen, Microcalorimetry of dust particles in a radio-frequency plasma, J. Appl. Phys. **88**, 1747 (2000).

[18] H. Maurer, R. Basner, and H. Kersten, Measuring the temperature of microparticles in plasmas, Rev. Sci. Instrum. **79**, 093508 (2008).

[19] T. Lopez and L. Mangolini, In situ monitoring of hydrogen desorption from silicon nanoparticles dispersed in a nonthermal plasma, J. Vac. Sci. Technol., B **34**, 041206 (2016).

[20] A. Woodard, K. Shojaei, G. Nava, and L. Mangolini, Graphitization of carbon particles in a non-thermal plasma reactor, Plasma Chem. Plasma Process. **38**, 683 (2018).

[21] S. G. Walton, B. M. Foley, J. Tomko, D. R. Boris, E. D. Gillman, S. C. Hernández, A. Giri, T. B. Petrova, and P. E.

Hopkins, Plasma-surface interactions in atmospheric pressure plasmas: In situ measurements of electron heating in materials, J. Appl. Phys. **124**, 043301 (2018).
[22] M. J. Allen, V. C. Tung, and R. B. Kaner, Honeycomb carbon: A review of graphene, Chem. Rev. **110**, 132 (2010).
[23] W. Choi, I. Lahiri, R. Seelaboyina, and Y. S. Kang, Synthesis of graphene and its applications: A review, Crit. Rev. Solid State Mater. Sci. **35**, 52 (2010).
[24] S. Dutta and S. K. Pati, Novel properties of graphene nanoribbons: A review, J. Mater. Chem. **20**, 8207 (2010).
[25] D. Akinwande, et al., A review on mechanics and mechanical properties of 2D materials—Graphene and beyond, Extreme Mech. Lett. **13**, 42 (2017).
[26] Y. Zhu, S. Murali, W. Cai, X. Li, J. W. Suk, J. R. Potts, and R. S. Ruoff, Graphene and graphene oxide: Synthesis, properties, and applications, Adv. Mater. **22**, 3906 (2010).
[27] A. A. Balandin, S. Ghosh, W. Bao, I. Calizo, D. Teweldebrhan, F. Miao, and C. N. Lau, Superior thermal conductivity of single-layer graphene, Nano Lett. **8**, 902 (2008).
[28] I. Calizo, A. A. Balandin, W. Bao, F. Miao, and C. N. Lau, Temperature dependence of the Raman spectra of graphene and graphene multilayers, Nano Lett. **7**, 2645 (2007).
[29] A. A. Balandin, Thermal properties of graphene and nanostructured carbon materials, Nat. Mater. **10**, 569 (2011).
[30] J. Hou, Y. Shao, M. W. Ellis, R. B. Moore, and B. Yi, Graphene-based electrochemical energy conversion and storage: Fuel cells, supercapacitors and lithium ion batteries, Phys. Chem. Chem. Phys. **13**, 15384 (2011).
[31] H.-J. Choi, S.-M. Jung, J.-M. Seo, D. W. Chang, L. Dai, and J.-B. Baek, Graphene for energy conversion and storage in fuel cells and supercapacitors, Nano Energy **1**, 534 (2012).
[32] L. Dai, Functionalization of graphene for efficient energy conversion and storage, Acc. Chem. Res. **46**, 31 (2013).
[33] F. Schedin, A. K. Geim, S. V. Morozov, E. W. Hill, P. Blake, M. I. Katsnelson, and K. S. Novoselov, Detection of individual gas molecules adsorbed on graphene, Nat. Mater. **6**, 652 (2007).
[34] H. J. Yoon, D. H. Jun, J. H. Yang, Z. Zhou, S. S. Yang, and M. M.-C. Cheng, Carbon dioxide gas sensor using a graphene sheet, Sens. Actuators, B **157**, 310 (2011).
[35] C. Huang, C. Li, and G. Shi, Graphene based catalysts, Energy Environ. Sci. **5**, 8848 (2012).
[36] B. F. Machado and P. Serp, Graphene-based materials for catalysis, Catal. Sci. Technol. **2**, 54 (2012).
[37] H. R. Byon, J. Suntivich, and Y. Shao-Horn, Graphene-based non-noble-metal catalysts for oxygen reduction reaction in acid, Chem. Mat. **23**, 3421 (2011).
[38] F. Schwierz, Graphene transistors, Nat. Nanotechnol. **5**, 487 (2010).
[39] T. Georgiou, R. Jalil, B. D. Belle, L. Britnell, R. V. Gorbachev, S. V. Morozov, Y.-J. Kim, A. Gholinia, S. J. Haigh, O. Makarovsky, L. Eaves, L. A. Ponomarenko, A. K. Geim, K. S. Novoselov, and A. Mishchenko, Vertical field-effect transistor based on graphene–WS_2 heterostructures for flexible and transparent electronics, Nat. Nanotechnol. **8**, 100 (2013).
[40] F. Kargar, Z. Barani, R. Salgado, B. Debnath, J. S. Lewis, E. Aytan, R. K. Lake, and A. A. Balandin, Thermal percolation threshold and thermal properties of composites with high loading of graphene and boron nitride fillers, ACS Appl. Mater. Interfaces **10**, 37555 (2018).
[41] Z. Barani, F. Kargar, K. Godziszewski, A. Rehman, Y. Yashchyshyn, S. Rumyantsev, G. Cywiński, W. Knap, and A. A. Balandin, Graphene epoxy-based composites as efficient electromagnetic absorbers in the extremely high-frequency band, ACS Appl. Mater. Interfaces **12**, 28635 (2020).
[42] Z. Barani, F. Kargar, A. Mohammadzadeh, S. Naghibi, C. Lo, B. Rivera, and A. A. Balandin, arXiv:2004.12201, (2020)
[43] K. M. F. Shahil and A. A. Balandin, Thermal properties of graphene and multilayer graphene: Applications in thermal interface materials, Solid State Commun. **152**, 1331 (2012).
[44] H. Shen, L. Zhang, M. Liu, and Z. Zhang, Biomedical applications of graphene, Theranostics **2**, 283 (2012).
[45] Y. Wang, Z. Li, J. Wang, J. Li, and Y. Lin, Graphene and graphene oxide: Biofunctionalization and applications in biotechnology, Trends Biotechnol. **29**, 205 (2011).
[46] S. Gilje, S. Han, M. Wang, K. L. Wang, and R. B. Kaner, A chemical route to graphene for device applications, Nano Lett. **7**, 3394 (2007).
[47] F. Perreault, A. Fonseca de Faria, and M. Elimelech, Environmental applications of graphene-based nanomaterials, Chem. Soc. Rev. **44**, 5861 (2015).
[48] E. Chávez-Ángel, J. S. Reparaz, J. Gomis-Bresco, M. R. Wagner, J. Cuffe, B. Graczykowski, A. Shchepetov, H. Jiang, M. Prunnila, J. Ahopelto, F. Alzina, and C. M. S. Torres, Reduction of the thermal conductivity in free-standing silicon nano-membranes investigated by non-invasive Raman thermometry, APL Mater. **2**, 012113 (2014).
[49] T. Beechem, A. Christensen, S. Graham, and D. Green, Micro-Raman thermometry in the presence of complex stresses in GaN devices, J. Appl. Phys. **103**, 124501 (2008).
[50] See Supplemental Material at http://link.aps.org/supplemental/10.1103/PhysRevApplied.15.024018 for a photograph of the reaction chamber.
[51] X. Li, W. Cai, J. An, S. Kim, J. Nah, D. Yang, R. Piner, A. Velamakanni, I. Jung, E. Tutuc, S. K. Banerjee, L. Colombo, and R. S. Ruoff, Large-area synthesis of high-quality and uniform graphene films on copper foils, Science **324**, 1312 (2009).
[52] X. Li, C. W. Magnuson, A. Venugopal, J. An, J. W. Suk, B. Han, M. Borysiak, W. Cai, A. Velamakanni, Y. Zhu, L. Fu, E. M. Vogel, E. Voelkl, L. Colombo, and R. S. Ruoff, Graphene films with large domain size by a two-step chemical vapor deposition process, Nano Lett. **10**, 4328 (2010).
[53] See Supplemental Material at http://link.aps.org/supplemental/10.1103/PhysRevApplied.15.024018 for a detailed description and a schematic of the optical set-up.
[54] A. C. Ferrari and J. Robertson, Interpretation of Raman spectra of disordered and amorphous carbon, Phys. Rev. B **61**, 14095 (2000).
[55] A. G. Souza Filho, A. Jorio, J. H. Hafner, C. M. Lieber, R. Saito, M. A. Pimenta, G. Dresselhaus, and

M. S. Dresselhaus, Electronic transition energy E_{ii} for an isolated (n,m) single-wall carbon nanotube obtained by anti-Stokes/Stokes resonant Raman intensity ratio, Phys. Rev. B **63**, 241404 (2001).

[56] H. Peng, N. B. M. Schröter, J. Yin, H. Wang, T.-F. Chung, H. Yang, S. Ekahana, Z. Liu, J. Jiang, L. Yang, T. Zhang, C. Chen, H. Ni, A. Barinov, Y. P. Chen, Z. Liu, H. Peng, and Y. Chen, Substrate doping effect and unusually large angle van hove singularity evolution in twisted Bi- and multilayer graphene, Adv. Mater. **29**, 1606741 (2017).

[57] See Supplemental Material at http://link.aps.org/supplemental/10.1103/PhysRevApplied.15.024018 for the detailed description of the heat transfer model.

[58] BOLSIG+ version 12/2017 was used for these calculations.

[59] See Supplemental Material at http://link.aps.org/supplemental/10.1103/PhysRevApplied.15.024018 for emission spectra at different power and gas compositions.

[60] S. Bellani, B. Martín-García, R. Oropesa-Nuñez, V. Romano, L. Najafi, C. Demirci, M. Prato, A. E. Del Rio Castillo, L. Marasco, E. Mantero, G. D'Angelo, and F. Bonaccorso, "Ion sliding" on graphene: A novel concept to boost supercapacitor performance, Nanoscale Horiz. **4**, 1077 (2019).

[61] See Supplemental Material at http://link.aps.org/supplemental/10.1103/PhysRevApplied.15.024018 for the detailed description of the method used to estimate the number of layers in our samples.

[62] G. López-Polín, C. Gómez-Navarro, V. Parente, F. Guinea, Mikhail I. Katsnelson, F. Pérez-Murano, and J. Gómez-Herrero, Increasing the elastic modulus of graphene by controlled defect creation, Nat. Phys. **11**, 26 (2015).

[63] L. Xie, L. Jiao, and H. Dai, Selective etching of graphene edges by hydrogen plasma, J. Am. Chem. Soc. **132**, 14751 (2010).